Inorganic Chemistry
Cite This: Inorg. Chem. 2018, 57, 3626−3633
Forum Article
pubs.acs.org/IC

Strategies toward the Enhanced Permeability and Retention Effect by Increasing the Molecular Weight of Arene Ruthenium Metallaassemblies

Vidya Mannancherril and Bruno Therrien*

Institut de Chimie, Université de Neuchâtel, Avenue de Bellevaux 51, 2000 Neuchâtel, Switzerland

Supporting Information

ABSTRACT: The enhanced permeability and retention (EPR) effect is an attractive avenue to target tumors: The size of the drug is the key to accumulating predominantly in tumors. Therefore, to increase the molecular weight of arene ruthenium metallaassemblies, several strategies can be adopted, and we present here our first step in the design of larger and heavier discrete arene ruthenium metallaassemblies to reach an EPR-size dimension.

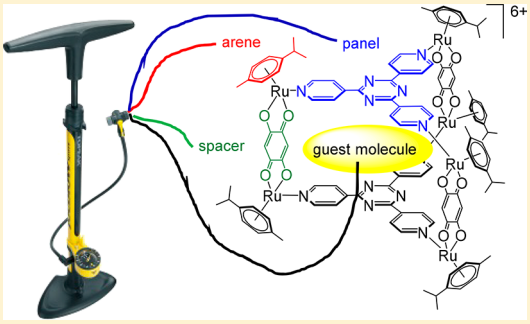

INTRODUCTION

Most solid and metastatic tumors show unique characteristics that are not observed in healthy tissues and organs, such as increased production of vascular permeability mediators, defective vascular architecture, impaired lymphatic drainage, and impaired recovery system, as well as an extensive angiogenesis, leading to a hypervasculature. All of these features compose the enhanced permeability and retention (EPR) effect.[1,2] Currently, only a small number of drugs are effective against metastatic cancers; therefore, the EPR effect offers great perspectives in nanomedicine therapy.

The EPR effect was first described in 1986 by Maeda, and it remains a popular strategy for cancer-selective drug delivery,[1,2] despite recent indications that the EPR effect might not be valid in humans.[3] Nevertheless, rapid and chaotic angiogenesis, coupled with the excessive production of vascular mediators, generates poorly defined blood vessels, showing gaps between endothelial cells.[1−4] Tumor blood vessels do not have a fixed and compact structure like healthy tissues but a very dynamic system with large openings between endothelial cells, which make them leaky and permeable. The size of those gaps can vary from 100 nm to approximately 1 μm, whereas in normal tissues, the gaps are <6 nm (continuous endothelial cells in striated muscles) and 10−100 nm in diameter (fenestrated endothelial cells in renal medulla, endocrine glands, renal glomerulus, choroid plexus in the brain, and intestinal villus) and even larger (discontinuous endothelial cells in sinusoidal vessels, liver, spleen, bone marrow, and extraneous particles from the blood).[5−7]

High-molecular-weight compounds such as nanoparticles, macromolecular drugs, polymeric drugs, and lipid particles enter predominantly into tumor tissues rather than into normal tissues (enhanced permeability) and will remain in the tumor for a prolonged period of time (retention). In Figure 1, the upper part shows healthy tissues, where the cellular structure is well-defined and where small molecules are able to pass the endothelial cells to enter and are subsequently removed by the lymphatic drainage. The lower part shows cancerous tissues with large gaps between cells, where not only small molecules but also macromolecules can enter. Furthermore, large molecules (drugs) will accumulate because of a defective lymphatic drainage.

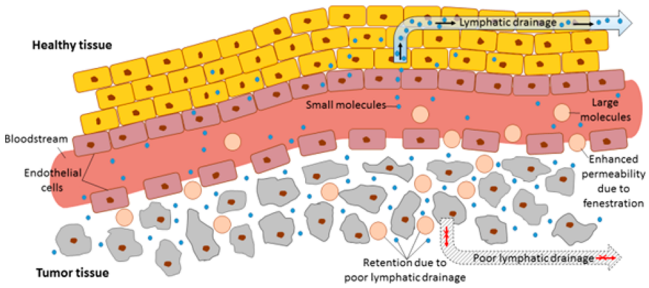

Figure 1. Illustration of the EPR effect: (top) healthy tissue; (bottom) tumor tissue.

A key mechanism of the EPR effect is the retention of high-molecular-weight substances in the tumor environment, whereas low-molecular-weight substances are returned to the blood circulatory system by diffusion.[1] Retention is caused by impaired lymphatic drainage. Intact lymphatic drainage ensures

Special Issue: Self-Assembled Cages and Macrocycles

Received: October 19, 2017
Published: December 22, 2017

DOI: 10.1021/acs.inorgchem.7b02668
Inorg. Chem. 2018, 57, 3626−3633

Table 1. Examples of Macromolecular Anticancer Drugs That Have Passed Clinical or Preclinical Trials

drug	active component	conjugate	mode of action
DaunoXome	daunorubicin (anthracycline)	daunorubicin citrate liposome	prevention of DNA replication, inhibition of protein synthesis, and conjugate decreases side effects[13]
Abraxane	paclitaxel (taxanes)	paclitaxel bound to albumin	blocks mitosis and one stade of cell division[14]
Genexol-PM	paclitaxel	paclilaxel-loaded polymeric micelle	antineoplastic activity, interferes with mitosis, and conjugate increases water solubility[15]
DepoCyte	cytarabine	cytarabine encapsulated in multivesicular lipid particles for sustained release (Depofaom)	antimetabolites that are similar to normal substances in the cell (when they are incorporated into the cellular metabolism, the cells are unable to divide[16])
Doxil	doxorubicin (anthracycline)	PEGylated liposomal doxorubicin hydrochloride	prevention of DNA replication, inhibition of protein synthesis, and conjugate improves drug penetration into tumors and decreases drug clearance[17]
Myocet	doxorubicin (anthracycline)	doxorubicin−hydrochlorid packed in liposomes	prevention of DNA replication, inhibition of protein synthesis, and conjugate decreases side effects[18]
Oncaspar Pegaspargase	L-asparaginase	PEG conjugated with L-asparginase	L-asparagine depletion blocks protein synthesis and cell proliferation[12,19]
Oncaspar Calaspargase Pegol	L-asparaginase	*E. coli*-derived L-asparagine II conjugated with succinimidyl carbonate monoethylene glycol	antineoplastic activity, L-asparagine depletion blocks protein synthesis and cell proliferation[12,19]

that ectopic substances are removed from tissues. However, in a damaged lymphatic system, only low-molecular-weight substances are removed and high-molecular-weight substances are retained. After administration of such high-molecular-weight compounds, it was shown that their concentration is 10−200 times higher in tumors than in normal tissues,[5] and this phenomenon can be used to our benefit.

However, great diversities exist among tumors, and the grade of the EPR effect observed can differ tremendously. Some tumors show a strong EPR effect and others only a limited effect, which can be demonstrated by arterial angiography using an X-ray lipid contrast agent.[2] The vascular permeability and grade of the EPR effect may also depend on the tumor type and may increase with the tumor size and growth rate, and it might be higher in the periphery than in the central region of the tumors.[8] Therefore, there is no uniform treatment of solid cancers exploiting the EPR effect, which ensures sufficient drug delivery to all tumor regions.[9]

The overproduction of vascular mediators, such as bradykinin, nitric oxide (NO), vascular endothelial growth factor, and carbon monoxide (CO), further enhances the permeability of tumors. This can be used for the augmentation of EPR-based tumor targeting, achieving more tumor accumulation of macromolecular drugs.[5] NO production is inevitable during tumor growth to maintain the supply of nutrients and oxygen. In the presence of NO scavengers, extravasation is significantly inhibited. CO is involved in many biological functions including vascular regulation, antiapoptosis, antiinflammation, and angiogenesis. CO is also found to increase the vascular permeability and blood flow and augment the EPR effect. Furthermore, the usage of CO donors can increase the grade of the EPR effect.[5] Another strategy to enhance the EPR effect is elevation of the systolic blood pressure via slow angiotensin II infusion.[10] Infusion of angiotensin II, a peptide hormone, leads to a tremendous increase of the blood flow in the tumor tissue without increasing the blood flow in normal tissues.[11]

In this regard, many macromolecular compounds containing clinically approved small molecular drugs linked to biologically relevant enzymes or proteins have been developed to exploit the EPR effect. In addition, polymer conjugates can increase the water solubility of those drugs, and therefore the effectiveness can also be enhanced. Polymer conjugation alters the biodistribution of low-molecular-weight drugs, thus enabling tumor-specific targeting.[12] Examples of EPR-targeting compounds under clinical trials or being clinically approved are presented in Table 1.

In the case of Oncaspar (Pegaspargase), the active component is the already large enzyme L-asparaginase, which causes an L-asparagine depletion that prevents protein synthesis and cell proliferation. The drug was further modified by PEGylation (Calaspargase Pegol), which is an important tool in the development of anticancer conjugates. PEGylation has proven to be useful for a variety of reasons:[12] (i) it increases the protein solubility and stability and reduces protein immunogenicity, (ii) it prevents the rapid clearance of small proteins, (iii) it is nontoxic and nonimmunogenic, (iv) it increases the plasma residence of the drug conjugate, (v) it can increase the therapeutic index in order to elevate the dose without causing toxicity, and (vi) its high degree of hydration provides a water shell to mask the active core. Overall, these commercial examples confirm that designing large conjugates to treat cancers is a suitable strategy.

Nevertheless, researchers disagree about the perfect size (20−200 nm)[3] or weight (25−160 kDa) for an EPR-effective drug. In the year 2000, Maeda stated that the EPR effect was observed at a molecular weight of 60 kDa, whereas later he stated that accumulation was observed already at a weight of 40 kDa.[1,2,10,20] In 2006, Haag and Kratz observed an EPR effect at a molecular weight of 20 kDa, but they also stated that the renal clearance occurs at a molecular weight of 30−50 kDa.[21] In 2014 Kobayashi estimated a desired size of over 6 nm in diameter, which is approximately the pore size of a glomerulus of the kidney, to avoid excretion.[22] Caliceti and Veronese stated in 2003 that renal clearance can be avoided from a molecular weight of 70 kDa, but molecules that exceed this size can be eliminated from the body by other pathways, such as liver uptake, proteolytic digestion, and clearance by the immune system.[23] However, one thing is certain: As the molecular size increases, systematic clearance decreases.

To investigate the molecular size dependence of drugs, Jain and co-workers have examined compounds between 25 and 160 kDa in a mice transplanted human colon adenocarcinoma model using the intravital fluorescence microscopy technique.[8] The permeability increased by a factor of 2 from 25 to 160 kDa. The transport of macromolecular compounds appears to

DOI: 10.1021/acs.inorgchem.7b02668
Inorg. Chem. 2018, 57, 3626−3633

occur by diffusion through the porous structure. Experiments with liposomes performed by the same group suggest that the cutoff size of the pores lies between 400 and 600 nm in diameter.[8]

According to these studies, arene ruthenium metallaassemblies, if they are big enough, could, in principle, exploit the EPR effect. For many years, we[24−27] as well as others[28−30] have synthesized numerous tetranuclear, hexanuclear, and octanuclear arene ruthenium metallaassemblies, and the first example of a biologically active system was published in 2008.[31] The complex-in-a-complex system $[(acac)_2Pt\subset Ru_6(p\text{-cymene})_6(tpt)_2(dhbq)_3]^{6+}$ was able to carry platinum acetylacetonate to cancer cells. This supramolecular system possesses several components (Figure 2) and has a molecular weight of

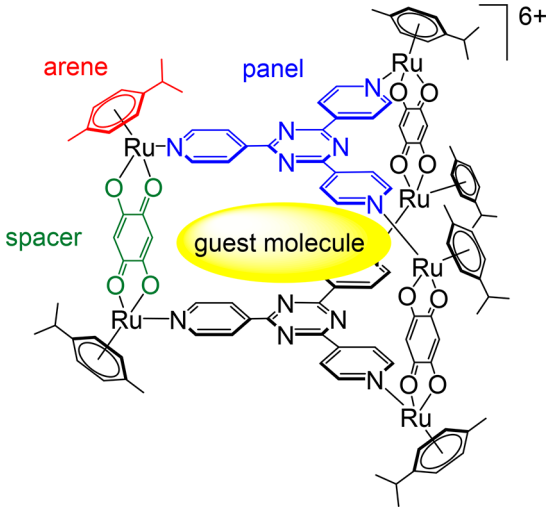

Figure 2. Components of a typical arene ruthenium metallaassembly.

approximately 4 kDa. The components are the arene ligands that can protect and stabilize the ruthenium atom in a 2+ oxidation state,[32] multidentate anionic spacers that can modulate the size of the cavity,[33] multidentate N-donor panels that can dictate the shape and geometry of the assembly.[34] All components can therefore be used to increase upon functionalization the molecular weight and size of the arene ruthenium metallaassemblies, including also the guest molecule.

Indeed, several pyrenyl-functionalized compounds have been used as guest molecules to increase the molecular weight of arene ruthenium metallaassemblies.[35,36] The pyrenyl group fits perfectly in the cavity of the metallaassemblies, while the remaining part sits outside (Figure 3). The hydrophobicity of pyrene coupled to the ideal shape of the cavity allows the formation of highly stable host−guest systems. As illustrated in Figure 3, when a large pyrenyl-functionalized guest is used, the arene ruthenium metallaassembly provides a cationic and hydrophilic head to the system. The largest host−guest system obtained so far has a combined (host−guest) molecular weight of 5.5 kDa.[37]

Until now, our efforts to increase the molecular weight of arene ruthenium metallaassemblies have mainly focused on the guest molecules. We want to explore now other possibilities such as the arenes, panels, and spacers. Herein, as a proof of concept, we present our preliminary study dealing with functionalized spacers, in which alkyl chains of different lengths are attached.

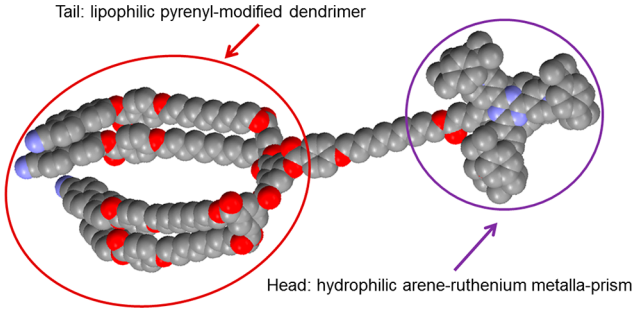

Figure 3. Pyrenyl-functionalized dendrimer encapsulated in an arene ruthenium metallaprism.

RESULTS AND DISCUSSION

To increase the molecular weight of arene ruthenium metallaassemblies, we have first focused our attention on the insertion of alkyl chains to the spacer components. Two types of spacers were chosen, dialkyloxalamide and 2,5-dihydroxy-3-alkyl-2,5-diene-1,4-dione (Figure 4). Synthetic strategies to

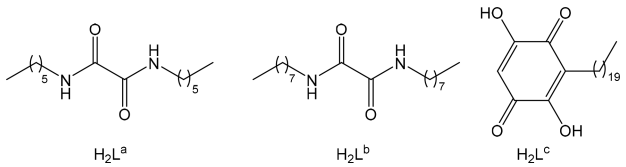

Figure 4. Spacers (H_2L) used in this study.

prepare such compounds are already available in the literature. Dihexyloxalamide (H_2L^a) and dioctyloxalamide (H_2L^b) were obtained following the strategy developed by Lu et al.,[38] while 2,5-dihydroxy-3-icosyl-2,5-diene-1,4-dione (H_2L^c) was prepared according to the method developed by Hu et al.,[39] by replacing a $C_{11}H_{23}$ alkyl chain with a $C_{20}H_{41}$ chain (see the Experimental Part). All compounds show the expected spectroscopic data and were used without further purification to synthesize the corresponding dinuclear arene ruthenium clip.

The dinuclear arene ruthenium metallaclips **1a** and **1b** (Scheme 1) are obtained in moderate yield by first reacting alkyloxalamides (H_2L^a and H_2L^b) with 2 equiv of *N,N*-

Scheme 1. Synthesis of the Dinuclear Arene Ruthenium Clips (1a−1c)

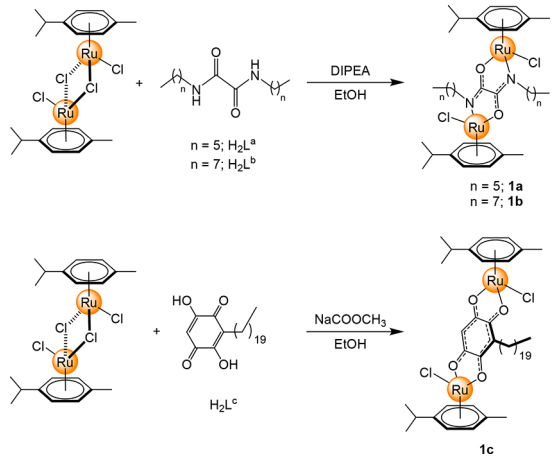

DOI: 10.1021/acs.inorgchem.7b02668
Inorg. Chem. 2018, 57, 3626−3633

diisopropylethylamine (DIPEA), followed by the addition of $[(\eta^6\text{-}p\text{-cymene})_2Ru_2(\mu_2\text{-}Cl)_2Cl_2]$. The metallaclip **1c** is prepared in good yield in a similar fashion, using $NaCOOCH_3$ as the base. All dinuclear complexes show in their ^1H NMR spectrum diastereotopic protons due to coordination of the arene ruthenium units to the spacers, with the ruthenium atoms being chiral-at-the-metal in these complexes.

Once the dinuclear clips have been prepared and purified, the synthesis of larger metallaassemblies was performed. A series of metallaprisms was obtained by reacting the dinuclear clips (**1**) with silver triflate, followed by the addition of 2,4,6-tripyridin-4-yl-1,3,5-triazine (4-tpt). These metallaprisms are isolated in good yield as dark-green (**2a** and **2b**) or dark-red (**2c**) solids (Figure 5). They are nonhygroscopic and stable in solution (dimethyl sulfoxide, dichloromethane, trichloromethane, and acetonitrile) for several days.

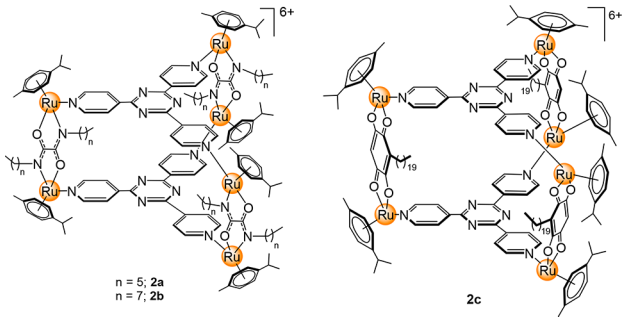

Figure 5. Molecular structures of the hexanuclear arene ruthenium metallaprisms (**2a**–**2c**).

The molecular structure of the metallaprisms was confirmed by a combination of NMR spectroscopy and mass spectrometry. Upon formation of the metallaprisms, the ^1H NMR signals assigned to the metallaclips are slightly shifted and become broad, while new signals associated with the 4-tpt panels appear (Figure 6). These observations are consistent

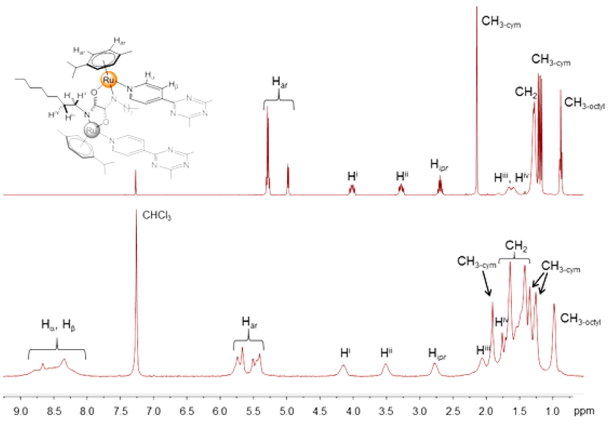

Figure 6. ^1H NMR spectra of **1b** (top) and **2b** (bottom).

with the formation of the metallaprisms **2a**–**2c**, in which the alkyl chains are either pointing away or toward the cavity and the components of the assemblies, thus generating large and broad signals.[40] Moreover, the nature of the metallaclips (**1a**–**1c**) generates two isomers for each metallaprism,[41] in which the orientations of the μ_4-L spacers are either all the same or mixed.

The electrospray ionization mass spectrometry (ESI-MS) spectra of the metallaprisms show characteristic dicationic ($[\mathbf{2} - 2CF_3SO_3^-]^{2+}$) and tricationic ($[\mathbf{2} - 3CF_3SO_3^-]^{3+}$) peaks, corresponding to the intact metallaprism plus four triflate and three triflate anions, respectively (Figure 7). Moreover, the

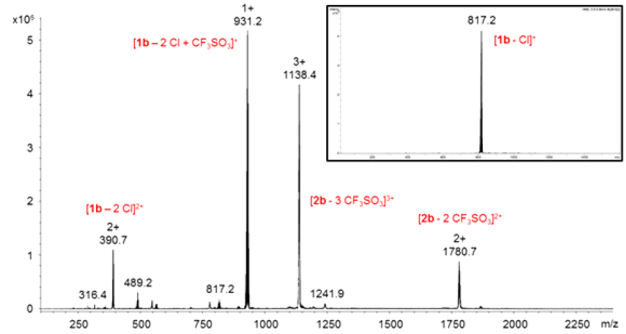

Figure 7. ESI-MS spectra of **1b** (inset) and **2b**.

dinuclear arene ruthenium clips show a single parent mass peak corresponding to $[\mathbf{1} - Cl]^+$, a peak not observed in the mass spectra of the metallaprisms. However, fragments corresponding to $[(p\text{cymene})_2Ru_2(\mu_4\text{-L})]^{2+}$ and $[(p\text{cymene})_2Ru_2(\mu_4\text{-L}) + CF_3SO_3]^+$ are observed in the mass spectra of **2** and confirmed the presence of the metallaclips in the metallaprisms. To illustrate this behavior, the mass spectra of **1b** and **2b** are presented in Figure 7.

Thus far, in this project, three prisms were synthesized. The molecular weights of the prisms amount to 3696.6 g mol^{-1} (**2a**), 3864.8 g mol^{-1} (**2b**), and 4191.0 g mol^{-1} (**2c**), still remaining relatively small to fully exploit the EPR effect. However, by the introduction of octyl chains on the oxalamide spacer, an additional mass of 589 g mol^{-1} was added to the metallaprism **2b**, in comparison to a dimethyloxalamide analogue. Unfortunately, attempts to introduce longer alkyl chains to the oxalamide moiety were unsuccessful, generating only insoluble materials. Nevertheless, by the simple addition of one icosyl chain to a dihydroxy benzoquinone spacer, a mass of nearly 1 kDa was added to the metallaprism, representing an increase of about 20% compared to the nonfunctionalized dihydroxybenzoquinone metallaprism (Figure 2).

As demonstrated here, the insertion of alkyl chains into organic spacers remains easy synthetically but reduces the solubility of the compounds. Therefore, to facilitate solubility while still increasing the molecular weight of the metallaassemblies, we are now shifting our attention to PEGylated chains, and instead of dealing with monofunctionalized hydroxybenzoquinone spacers, we are preparing bis-functionalized derivatives.[42]

CONCLUSION

The EPR effect represents an important discovery that occurs in most solid cancers. This phenomenon is based on the cellular structure of solid cancers and on defective lymphatic drainage. Macromolecular compounds can be administered in order to accumulate on tumor sites and to operate locally via the EPR effect. However, to date, no ruthenium-containing drugs are known to operate via the EPR effect, and studies have shown that the EPR effect is questionable when dealing with humans.[3]

Therefore, if reaching an EPR effect is no longer a goal, these functionalized arene ruthenium metallaassemblies can still find

DOI: 10.1021/acs.inorgchem.7b02668
Inorg. Chem. 2018, 57, 3626–3633

other applications, such as drug-delivery vectors. Indeed, the use of metallacages as drug-delivery vectors and as anticancer agents is becoming a new field of research, showing great promise.[43−45] Then, like in arene ruthenium metallaassemblies, the introduction of tumor-targeting agents at the periphery of the metallaassembly can, in principle, increase the selectivity and efficacy of these abiological systems.[46]

For these reasons, we want in the future to use similar synthetic strategies to functionalize as well the arenes and panels and not only the spacers and guest molecules. We also want to use other metals (iridium or osmium) and introduce specific functional groups (targeting agents, hydrophilic or hydrophobic groups, peptidic chains, etc.) to fine-tune the biological activity and, ultimately, to generate metallaassemblies with higher and better therapeutic properties (Figure 8).

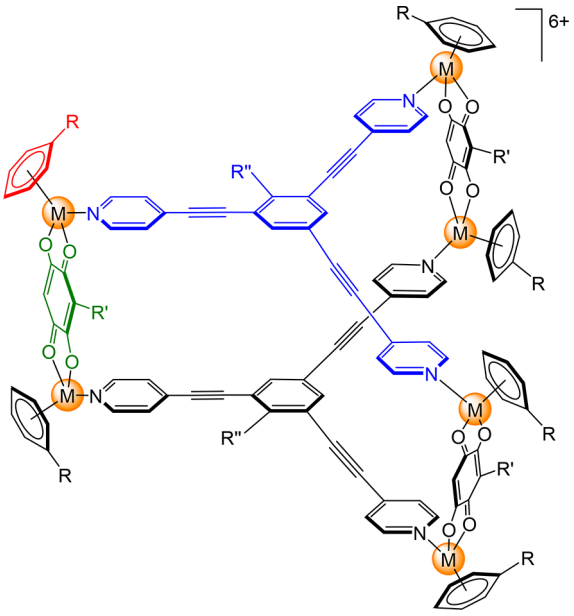

Figure 8. Highly functionalized metallaassemblies.

EXPERIMENTAL PART

Materials and Methods. All solvents were dried before use according to standard procedures, and all reactions were performed under an inert atmosphere. All other reagents were commercially available and were used as received. NMR spectra were recorded with a Bruker Avance II 400 spectrometer. UV−vis absorption spectra were recorded with a PerkinElmer UV−vis spectrophotometer. IR spectra were recorded with a Thermoscientific Nicolet iS5 spectrometer. Electrospray ionization mass spectrometry (ESI-MS) spectra were obtained in positive or negative mode with a LCQ Finnigan mass spectrometer. Microanalyses were carried out by the Mikroelementaranalytisches Laboratorium, ETH Zürich (Zürich, Switzerland). The ruthenium precursor $[(\eta^6\text{-}p\text{-cymene})_2Ru_2(\mu_2\text{-}Cl)_2Cl_2]$,[47] the spacers dihexyloxalamide (H_2L^a)[38] and dioctyloxalamide (H_2L^b),[38] and the panel ligand 2,4,6-tripyridin-4-yl-1,3,5-triazine (4-tpt)[48] were prepared according to published methods.

Synthesis of 3-Icosyl-1,2,4,5-tetramethoxybenzene. 1,2,3,4-Tetramethoxybenzene (430 mg, 2.20 mol, 1.0 equiv) was dissolved in tetrahydrofuran (10 mL), and the solution was cooled to −10 °C. The flask was flushed with N_2, and *n*-BuLi (2.5 M in hexane, 1 mL, 2.42 mmol, 1.1 equiv) was slowly added under a N_2 atmosphere. The mixture was stirred at −10 °C for 30 min, and 1-bromoicosane (904 mg, 2.42 mmol, 1.1 equiv) was slowly added. The mixture was stirred at −10 °C for 10 min and then allowed to warm to room temperature (RT) overnight. After completion of the reaction, aqueous saturated NH_4Cl (2 mL) was added to the solution, and the mixture was extracted with Et_2O (3 × 50 mL), washed with brine (1 × 50 mL), dried over $MgSO_4$, filtered, and concentrated under reduced pressure. The crude product was purified by flash column chromatography (SiO_2 and 40:1 pentane/EtOAc) to yield the desired product as a colorless solid (710 mg, 68%). ^{1}H NMR ($CDCl_3$, 400 MHz): δ 6.41 (s, 1H, C*H*), 3.84 (s, 6H, OCH_3), 3.76 (s, 6H, OCH_3), 2.62−2.59 (m, 2H, CH_2), 1.56−1.49 (m, 2H, CH_2), 1.37−1.35 (m, 2H, CH_2), 1.25 (s, 32H, CH_2), 0.88 (t, $^3J_{HH}$ = 6.2 Hz, 3H, CH_3). ^{13}C NMR ($CDCl_3$, 101 MHz): δ 149.0 (2C, CH_3OC), 141.3 (2C, CH_3OC), 131.3 (1C, $CC_{20}H_{41}$), 96.9 (1C, *C*H), 61.1 (2C, OCH_3), 56.4 (2C, OCH_3), 32.1 (1C, CH_2), 30.9 (1C, CH_2), 30.2 (1C, CH_2), 29.9 (10C, CH_2), 29.8 (1C, CH_2), 29.7 (1C, CH_2), 29.6 (1C, CH_2), 29.5 (1C, CH_2), 24.8 (1C, CH_2), 22.8 (1C, CH_2), 14.3 (1C, CH_3). IR (cm^{-1}): 2957 (w), 2916 (m), 2849 (m), 1594 (w), 1467 (m), 1408 (m), 1367 (w), 1343 (w), 1306 (w), 1244 (w), 1203 (w), 1117 (m), 1066 (w), 1044 (m), 1024 (w), 954 (m), 899 (w), 868 (w), 854 (w), 831 (W), 811 (w), 721 (w), 639 (w). ESI-MS$^+$. Calcd for $C_{30}H_{54}O_4Na$ ([M + Na]$^+$): *m*/*z* 501.4. Found: *m*/*z* 501.4. UV−vis [1.0 × 10^{-4}, CH_2Cl_2; λ_{max}, nm (ε, M^{-1} cm^{-1})]: 229 (0.7 × 10^3), 284 (1.7 × 10^3). Elem anal. Calcd for $C_{30}H_{54}O_4$ (478.4): C, 75.26; H, 11.37. Found: C, 75.40; H, 11.39.

Synthesis of 3-Icosyl-2,5-dimethoxycyclohexa-2,5-diene-1,4-dione. 3-Icosyl-1,2,4,5-tetramethoxybenzene (177 mg, 370 μmol, 1.0 equiv) was suspended in acetonitrile (3 mL), ceric ammonium nitrate (510 mg, 930 μmol, 2.51 equiv) was added, and the yellow suspension turned into an orange suspension. The mixture was stirred at RT for 2 h. After completion of the reaction, the mixture was extracted with EtOAc (3 × 15 mL). The combined organic layers were washed with brine (1 × 20 mL), dried over $MgSO_4$, filtered, and concentrated under reduced pressure. The crude product was purified by flash column chromatography (SiO_2 and 20:1 pentane/EtOAc) to yield the desired product as a colorless solid (80.2 mg, 48%). ^{1}H NMR ($CDCl_3$, 400 MHz): δ 5.72 (s, 1H, C*H*), 4.04 (s, 3H, OCH_3), 3.80 (s, 3H, OCH_3), 2.42 (t, $^3J_{HH}$ = 7.5 Hz, 2H, CH_2), 1.41−1.35 (m, 2H, CH_2), 1.25 (s, 34 H, CH_2), 0.88 (t, $^3J_{HH}$ = 6.6 Hz, 3H, CH_3). ^{13}C NMR ($CDCl_3$, 101 MHz): δ 183.7 (1C, *C*O), 182.6 (1C, *C*O), 158.9 (1C, CH_3OC), 156.0 (1C, CH_3OC), 130.9 (1C, $CC_{20}H_{41}$), 105.5 (1C, *C*H), 61.5 (1C, OCH_3), 56.5 (1C, OCH_3), 32.1 (1C, CH_2), 29.8 (8C, CH_2), 29.75 (4C, CH_2), 29.68 (1C, CH_2), 29.55 (1C, CH_2), 29.51 (1C, CH_2), 28.82 (1C, CH_2), 23.2 (1C, CH_2), 22.8 (1C, CH_2), 14.3 (1C, CH_3). IR (cm^{-1}): 2916 (m), 2849 (m), 1649 (w), 1597 (w), 1467 (w), 1324 (w), 1206 (w), 1154 (w), 1046 (w), 928 (w), 835 (w), 797 (w), 720 (w), 500 (w), 483 (w), 469 (w), 401 (w), 453 (w), 433 (w), 429 (w). MS (ESI$^+$). Calcd for $C_{28}H_{48}O_4Na$ ([M + Na]$^+$): *m*/*z* 471.4. Found: *m*/*z* 471.3. UV−vis [1.0 × 10^{-4}, CH_2Cl_2; λ_{max}, nm (ε, M^{-1} cm^{-1})]: 286 (8.2 × 10^3). Elem anal. Calcd for $C_{28}H_{48}O_4$ (448.4): C, 74.95; H, 10.78. Found: C, 75.21; H, 10.85.

Synthesis of 2,5-Dihydroxy-3-icosylcyclohexa-2,5-diene-1,4-dione (H_2L^c). 3-Icosyl-2,5-dimethoxycyclohexa-2,5-diene-1,4-dione (116 mg, 259 μmol, 1.0 equiv) and ethanol (EtOH; 10 mL) were mixed to give an orange suspension. NaOH (2 M, 5 mL) was added, and the suspension turned into a violet solution. The solution was heated to 70 °C and stirred until thin-layer chromatography showed full conversion of the starting material. The reaction was allowed to cool to RT, HCl (2 M, 25 mL) was added, and the solution turned into an orange suspension. The mixture was extracted with EtOAc (3 × 30 mL). The combined organic layers were dried over $MgSO_4$, filtered, concentrated, and dried under high vacuum to yield the desired product as a brown solid, which was used without further purification (73 mg, 72%). ^{1}H NMR ($SO(CD_3)_2$, 400 MHz): δ 11.17 (s, 2H, O*H*), 5.77 (s, 1H, C*H*), 2.27 (t, $^3J_{HH}$ = 7.5 Hz, 2H, CH_2), 1.34 (m, 2H, CH_2), 1.22 (m, 34H, CH_2), 0.84 (t, $^3J_{HH}$ = 6.6 Hz, 3H, CH_3). IR (cm^{-1}): 3304 (m), 2917 (m), 2847 (m), 1612 (m), 1462 (w), 1325 (m), 1187 (m), 860 (w), 768 (w), 708 (w). MS (ESI$^-$). Calcd for $C_{26}H_{43}O_4$ ([M − H]$^-$): *m*/*z* 419.3. Found: *m*/*z* 419.3. UV−vis [1.0 × 10^{-4}, CH_2Cl_2; λ_{max}, nm (ε, M^{-1} cm^{-1})]: 282 (1.4 × 10^4), 290 (1.4 × 10^4).

*Synthesis of the Metallaclip $[(\eta^6\text{-}p\text{-Cymene})_2Ru_2(\mu_4\text{-}L^a)Cl_2]$ (**1a**).* H_2L^a (200 mg, 780 μmol, 1.0 equiv) was suspended in EtOH (15

DOI: 10.1021/acs.inorgchem.7b02668
Inorg. Chem. 2018, 57, 3626−3633

mL), and DIPEA (0.3 mL, 1.73 mmol, 2.2 equiv) was added dropwise at RT. The mixture was heated to 50 °C until the solid was dissolved, and the solution was stirred at that temperature for 30 min. The dinuclear complex $[(\eta^6\text{-}p\text{-cymene})_2Ru_2(\mu_2\text{-Cl})_2Cl_2]$ (500 mg, 0.816 mmol, 1.05 equiv) was added, and the mixture was heated at 80 °C overnight. The mixture was allowed to cool to RT, filtered, washed with EtOH, acetone, H_2O, Et_2O, and pentane, and then dissolved in CH_2Cl_2, before being filtered over Celite and concentrated under reduced pressure to yield the desired product as an orange solid (156 mg, 25%). ^{1}H NMR ($CDCl_3$, 400 MHz): δ 5.31−5.26 (m, 6H, C*H*), 4.99 (d, $^3J_{HH}$ = 5.9 Hz, 2H, C*H*), 4.06−3.99 (m, 2H, C*H*H), 3.32−3.26 (m, 2H, C*H*H), 2.69 (sept, $^3J_{HH}$ = 6.9 Hz, 2H, C*H*), 2.15 (s, 6H, CH_3), 1.71−1.56 (m, 4H, CH_2), 1.38−1.27 (m, 12H, CH_2), 1.22 (d, $^3J_{HH}$ = 6.9 Hz, 6H, CH_3), 1.18 (d, $^3J_{HH}$ = 6.9 Hz, 6H, CH_3), 0.92−0.87 (m, 6H, CH_3). ^{13}C NMR ($CDCl_3$, 101 MHz): δ 170.2 (2C, *C*O), 100.7 (2C, *C*CH(CH_3)$_2$), 94.4 (2C, *C*CH_3), 82.6 (2C, *C*H), 81.2 (2C, *C*H), 79.8 (2C, *C*H), 79.6 (2C, *C*H), 51.7 (2C, H*C*(CH_3)$_2$), 31.9 (2C, *C*H_2), 30.9 (2C, *C*H_2), 29.4 (2C, *C*H_2), 27.6 (2C, *C*H_2), 22.9 (2C, *C*H_2), 22.6 (2C, HC(*C*H_3)$_2$), 22.2 (2C, HC(*C*H_3)$_2$), 18.6 (2C, *C*H_3), 14.3 (2C, *C*H_3). IR (cm^{-1}): 2923 (w), 1596 (s), 1458 (w), 1333 (m), 1051 (w), 872 (w), 532 (w), 524 (w), 511 (w), 501 (w), 494 (w), 485 (w), 475 (w), 467 (w), 458 (w), 450 (w), 441 (w), 433 (w). MS (ESI$^+$). Calcd for $C_{34}H_{54}ClN_2O_2Ru_2$ ([M − Cl]$^+$): m/z 761.2. Found: m/z 761.1. UV−vis [1.0×10^{-5}, CH_2Cl_2; λ_{max}, nm (ε, M^{-1} cm^{-1})]: 231 (2.1×10^5). Elem anal. Calcd for $C_{34}H_{54}Cl_2N_2O_2Ru_2$ (795.9): C, 51.31; H, 6.84; N, 3.52. Found: C, 51.32; H, 6.85; N, 3.72.

*Synthesis of the Metallaclip $[(\eta^6\text{-}p\text{-Cymene})_2Ru_2(\mu_4\text{-}L^b)Cl_2]$ (**1b**).* H_2L^b (500 mg, 1.60 mmol, 1.0 equiv) was suspended in EtOH (30 mL), and DIPEA (0.6 mL, 3.44 mmol, 2.1 equiv) was added slowly and stirred at RT for 30 min. The dinuclear complex $[(\eta^6\text{-}p\text{-cymene})_2Ru_2(\mu_2\text{-Cl})_2Cl_2]$ (1.03g, 1.68 mmol, 1.05 equiv) was added, and the mixture was heated at 90 °C overnight. The reaction was allowed to cool to RT, the volume was reduced to half, and the mixture was stored in the refrigerator for 1 h. The orange residue was filtered and washed with EtOH, H_2O, acetone, Et_2O, and pentane. The residue was dissolved in CH_2Cl_2, filtered over Celite, and concentrated under reduced pressure to yield the desired product as an orange solid (280 mg, 21%). ^{1}H NMR ($CDCl_3$, 400 MHz): δ 5.30−5.25 (m, 6H, C*H*), 4.97 (d, $^3J_{HH}$ = 5.8 Hz, 2H, C*H*), 4.04−3.97 (m, 2H, C*H*H), 3.30−3.24 (m, 2H, C*H*H), 2.68 (sept, $^3J_{HH}$ = 6.9 Hz, 2H, C*H*), 2.12 (s, 6H, CH_3), 1.70−1.52 (m, 4H, CH_2), 1.33−1.25 (m, 20H, CH_2), 1.20 (d, $^3J_{HH}$ = 6.8 Hz, 6H, CH_3), 1.16 (d, $^3J_{HH}$ = 6.9 Hz, 6H, CH_3), 0.89−0.86 (m, 6H, CH_3). ^{13}C NMR ($CDCl_3$, 101 MHz): δ 170.1 (2C, *C*O), 100.7 (2C, *C*CH(CH_3)$_2$), 94.4 (2C, *C*CH_3), 82.5 (2C, *C*H), 81.2 (2C, *C*H), 79.7 (2C, *C*H), 79.5 (2C, *C*H), 51.7 (2C, H*C*(CH_3)$_2$), 32.1 (2C, *C*H_2), 30.7 (2C, *C*H_2), 29.7 (2C, *C*H_2), 29.5 (2C, *C*H_2), 29.4 (2C, *C*H_2), 27.9 (2C, *C*H_2), 22.8 (2C, *C*H_2), 22.6 (2C, HC(*C*H_3)$_2$, 22.2 (2C, HC(*C*H_3)$_2$), 18.6 (2C, *C*H_3), 14.3 (2C, *C*H_3). IR (cm^{-1}): 3302 (w), 2954 (m), 2914 (m), 2849 (m), 1645 (w), 1604 (s), 1531 (w), 1510 (w), 1466 (w), 1373 (w), 1349 (w), 1324 (m), 1200 (w), 1153 (w), 1080 (w), 1055 (w), 1025 (w), 996 (w), 857 (m), 800 (m), 724 (m), 594 (w), 496 (w), 463 (w), 445 (w), 429 (w). MS (ESI$^+$). Calcd for $C_{38}H_{62}ClN_2O_2Ru_2$ ([M − Cl]$^+$): m/z 817.3. Found: m/z 817.2. UV−vis [1.0×10^{-4}, CH_2Cl_2; λ_{max}, nm (ε, M^{-1} cm^{-1})]: 228 (2.33×10^4), 313 (1.6×10^4). Elem anal. Calcd for $C_{38}H_{62}N_2O_2Cl_2Ru_2$ (852.2): C, 53.57; H, 7.33; N, 3.29. Found: C, 53.61; H, 7.48; N, 3.24.

*Synthesis of the Metallaclip $[(\eta^6\text{-}p\text{-Cymene})_2Ru_2(\mu_4\text{-}L^c]Cl_2$ (**1c**).* H_2L^c (158 mg, 375 μmol, 1.0 equiv) was suspended in EtOH (50 mL), and $NaCOOCH_3$ (64.7 mg, 789 μmol, 2.1 equiv) was added. The yellow suspension turned into a red solution. The mixture was allowed to stir for 1 h at RT, then $[(\eta^6\text{-}p\text{-cymene})_2Ru_2(\mu_2\text{-Cl})_2Cl_2]$ (225 mg, 367 μmol, 0.98 equiv) was added, and the reaction was heated to 80 °C for 48 h. The reaction was allowed to cool to RT, the volume was reduced to half, and the mixture was stored in the refrigerator overnight. The violet precipitate was filtered and washed with cold H_2O to obtain the desired product as a violet solid (267 mg, 77%). ^{1}H NMR ($CDCl_3$, 400 MHz): δ 5.69 (s, 1H, C*H*), 5.63−5.59 (m, 4H, C*H*), 5.36 (d, $^3J_{HH}$ = 5.8 Hz, 4H, C*H*), 2.90 (sept, $^3J_{HH}$ = 6.9 Hz, 2H, C*H*), 2.36−2.32 (m, 2H, CH_2), 2.91 (s, 6H, CH_3), 1.36−1.33 (m, 12H, (CH_3)$_2$), 1.27−1.26 (m, 36H, CH_2), 0.89−0.86 (m, 3H, CH_3). ^{13}C NMR ($CDCl_3$, 101 MHz): δ 184.4 (2C, CO), 181.8 (2C, CO), 115.5 (1C, $CC_{20}H_{41}$), 100.7 (1C, CH), 100.6 (2C, $CCH(CH_3)_2$), 96.4 (2C, CCH_3), 82.0 (1C, CH), 81.4 (1C, CH), 79.7 (1C, CH), 79.1 (1C, CH), 32.1 (1C, CH_2), 31.5 (1C, CH_2), 30.0 (1C, CH_2), 30.0 (2C, CH_2), 29.9 (2C, CH), 29.9 (2C, CH_2), 29.9 (2C, CH_2), 29.9 (4C, CH_2), 29.8 (1C, CH_2), 29.7 (1C, CH_2), 29.5 (1C, CH_2), 28.3 (1C, CH_2), 22.8 (1C, CH_2), 22.7 (2C, (CH_3)$_2$), 18.7 (1C, CH_3), 14.3 (1C, CH_3). IR (cm^{-1}): 2918 (m), 2849 (m), 1509 (s), 1495 (s), 1469 (m), 1363 (s), 1315 (w), 1236 (w), 1225 (w), 1165 (w), 1086 (w), 1030 (w), 874 (w), 834 (w), 805 (w), 788 (w), 722 (w), 502 (w), 487 (w), 464 (w), 453 (w), 449 (w), 445 (w), 433 (w), 430 (w). MS (ESI$^+$). Calcd for $C_{46}H_{70}ClO_4Ru_2$ ([M − Cl]$^+$): m/z 925.3. Found: m/z 925.3. UV−vis [1.0×10^{-5}, CH_2Cl_2; λ_{max}, nm (ε, M^{-1} cm^{-1})]: 228 (3.7×10^4), 317 (1.5×10^4), 500 (2.0×10^4). Elem anal. Calcd for $C_{46}H_{70}O_4Cl_{12}Ru_2$ (960.3): C, 57.55; H, 7.35; N, 0.00. Found: C, 58.08; H, 7.56; N, 0.01.

*Syntheses of the Metallaprism $[(\eta^6\text{-}p\text{-Cymene})_6Ru_6(\mu_4\text{-}L^a)_3(\mu_3\text{-}4\text{-tpt})_2][CF_3SO_3]_6$ (**2a**).* The metallaclip **1a** (100 mg, 128 μmol, 1.0 equiv) was dissolved in methanol (MeOH; 20 mL), and $AgCF_3SO_3$ (64.0 mg, 249 μmol, 1.95 equiv) was added. The mixture was stirred at RT for 3 h. AgCl was filtered off, 4-tpt (44.0 mg, 141 μmol, 1.1 equiv) was added to the solution, and the mixture was heated at 60 °C for 24 h. The reaction was allowed to cool to RT, and the solvent was removed under reduced pressure. CH_2Cl_2 (2 mL) and pentane (100 mL) were added to induce precipitation. The dark-green precipitate was filtered and washed with cold EtOH (3 × 20 mL) to yield the desired product as a dark-green solid. (152 mg, 96%). ^{1}H NMR ($CDCl_3$, 400 MHz): δ 8.99−8.20 (m, 24H, C*H*), 5.83−5.69 (m, 12H, C*H*), 5.56−5.44 (m, 12H, C*H*), 4.20−4.13 (m, 6H, CH_2), 3.62−3.55 (m, 6H, CH_2), 2.86−2.75 (m, 6H, CH_2), 2.14−2.07 (m, 6H, CH_2), 1.96 (s, 18H, CH_3), 1.82−1.66 (m, 22H, CH_2), 1.61−1.52 (m, 20H, CH_2), 1.40−1.37 (m, 18H, CH_3), 1.32−1.26 (m, 18H, CH_3), 1.07−1.03 (m, 18H, CH_3). IR (cm^{-1}): 2928 (w), 1596 (s), 1516 (s), 1371 (m), 1257 (s), 1222 (m), 1149 (m), 1056 (w), 1028 (s), 811 (m), 670 (w), 636 (s), 496 (w), 480 (w), 445 (w). MS (ESI$^+$). Calcd for $C_{141}H_{186}F_9N_{18}O_{15}Ru_6S_3$ ([M − $3CF_3SO_3$]$^{3+}$): m/z 1083.3. Found: m/z 1082.4. Calcd for $C_{142}H_{186}F_{12}N_{18}O_{18}Ru_6S_4$ ([M − $2CF_3SO_3$]$^{2+}$): m/z 1699.4. Found: m/z 1697.3. UV−vis [1.0×10^{-5}, CH_2Cl_2; λ_{max}, nm (ε, M^{-1} cm^{-1})]: 249 (1.73×10^5). Elem anal. Calcd for $C_{144}H_{186}F_{18}N_{18}O_{24}Ru_6S_6$ (3696.6): C, 46.82; H, 5.08; N, 6.83. Found: C, 46.71; H, 5.12; N, 7.30.

*Syntheses of the Metallaprism $[(\eta^6\text{-}p\text{-Cymene})_6Ru_6(\mu_4\text{-}L^b)_3(\mu_3\text{-}4\text{-tpt})_2][CF_3SO_3]_6$ (**2b**).* The metallaclip **1b** (150 mg, 176 μmol, 1.0 equiv) was dissolved in MeOH (20 mL), and $AgCF_3SO_3$ (88.1 mg, 343 μmol, 1.95 equiv) was added. The mixture was stirred at RT for 3 h. AgCl was filtered off, 4-tpt (60.4 mg, 194 μmol, 1.1 equiv) was added to the mixture, and the solution was heated at 60 °C for 24 h. The reaction was allowed to cool to RT, and MeOH was removed. CH_2Cl_2 (2 mL) was added, and the pentane (100 mL) was added to induce precipitation. The dark-green-black precipitate was filtered and washed with EtOH (3 × 20 mL) to yield the desired product (129 mg, 60%). ^{1}H NMR ($CDCl_3$, 400 MHz): δ 8.78−8.21 (m, 24H, C*H*), 5.77−5.65 (m, 12H, C*H*), 5.51−5.39 (m, 12H, C*H*), 4.26−4.07 (m, 6H, CH_2), 3.60−3.42 (m, 6H, CH_2), 2.85−2.69 (m, 6H, CH_2), 2.13−2.00 (m, 8H, CH_2), 1.96−1.86 (m, 18H, CH_3), 1.79−1.74 (m, 4H, CH_2), 1.70−1.60 (m, 30H, CH_2), 1.48−1.34 (m, 44H, CH_2; CH_3), 1.30−1.19 (m, 22H, CH_2; CH_3), 1.06−0.92 (m, 18H, CH_3). IR (cm^{-1}): 2926 (w), 1596 (s), 1517 (s), 1466 (w), 1371 (m), 1332 (w), 1257 (s), 1222 (m), 1149 (m), 1056 (w), 1028 (s), 871 (w), 811 (m), 753 (w), 670 (w), 658 (w), 635 (s), 572 (w), 487 (w), 467 (w), 439 (w). MS (ESI$^+$). Calcd for $C_{153}H_{210}F_9N_{18}O_{15}Ru_6S_3$ ([M − $3CF_3SO_3$]$^{3+}$): m/z 1139.3. Found: m/z 1138.4. Calcd for $C_{154}H_{210}F_{12}N_{18}O_{18}Ru_6S_4$ ([M − $2CF_3SO_3$]$^{2+}$): m/z 1782.5. Found: m/z 1780.7. UV−vis [1.0×10^{-5}, CH_2Cl_2; λ_{max}, nm (ε, M^{-1} cm^{-1})]: 251 (1.33×10^5). Elem anal. Calcd for $C_{156}H_{210}F_{18}F_{18}O_{24}Ru_6S_6$ (3864.8): C, 48.51; H, 5.48; N, 6.53. Found: C, 48.31; H, 5.42; N, 7.76.

DOI: 10.1021/acs.inorgchem.7b02668
Inorg. Chem. 2018, 57, 3626−3633

*Synthesis of the Metallaprism [(η^6-p-Cymene)$_6$Ru$_6$(μ_4-L^c)$_3$(μ_3-4-tpt)$_2$][CF$_3$SO$_3$]$_6$ (**2c**).* The metallaclip **1c** (50.0 mg, 52.0 μmol, 1.0 equiv) was suspended in MeOH (20 mL), and $AgCF_3SO_3$ (26.7 mg, 104 μmol, 2.0 equiv) was added and the mixture was stirred at RT for 3 h. AgCl was filtered off and 4-tpt (10.7 mg, 34.3 μmol, 0.66 equiv) was added, and the mixture heated to 60 °C. The reaction was stirred for 30 h until the ^{1}H NMR spectrum showed full conversion of the starting material. Then, the reaction was allowed to cool to RT, the solvent was removed under reduced pressure, and the crude product was dried overnight. CH_2Cl_2 (1 mL) was added to dissolve the solid, and pentane (50 mL) was added to induce precipitation. The dark-red solid was filtered and dried under vacuum (56.7 mg, 60%). ^{1}H NMR ($CDCl_3$, 400 MHz): δ 8.75 (s, 12 H, C*H*), 8.49 (s, 12H, C*H*), 5.88−5.68 (m, 35 H, C*H*), 2.85 (m, 6H, C*H*), 2.28−2.17 (m, 36H, (CH_3)$_2$), 1.37−1.27 (132H, CH_2; CH_3), 0.88 (m, 9H, CH_3). ^{13}C NMR ($CDCl_3$, 101 MHz): δ 184.1 (6C, CO), 181.7 (6C, CO), 169.7, (6C, NCN), 154.2 (6C, CCC), 144.3 (12C, NCC), 125.6 (12C, CCC), 122.4 (3C, $CC_{20}H_{41}$), 119.2 (3C, CH), 104.4 (12C, CH), 99.1 (12C, CH), 84.1 (6C, $CCH(CH_3)_2$), 82.4 (6C, CCH_3), 32.1 (1C, CH_2), 31.5 (1C, CH_2), 30.2 (1C, CH_2), 30.1 (1C, CH), 30.1 (1C, CH_2), 30.0 (1C, CH_2), 30.0 (2C, CH_2), 29.9 (2C, CH_2), 29.8 (4C, CH_2), 29.5 (2C, CH_2), 22.8 (2C, $(CH_3)_2$), 22.9 (1C, CH_2), 22.5 (1C, CH_2), 22.4 (1C, CH_2), 18.2 (1C, CH_3), 14.3 (1C, CH_3). IR (cm^{-1}): 2924 (w), 2852 (w), 1575 (w), 1514 (m), 1367 (m), 1278 (m), 1243 (m), 1224 (m), 1156 (m), 1058 (w), 1027 (m), 870 (w), 810 (w), 800 (w), 759 (w), 671 (w), 667 (w), 635 (w), 487 (w), 472 (w), 464 (w), 453 (w). UV−vis [1.0×10^{-5}, CH_2Cl_2; λ_{max}, nm (ε, M^{-1} cm^{-1})]: 245 (7.8×10^4), 304 (4.3×10^4), 494 (2.8×10^4). MS (ESI$^+$). Calcd for $C_{177}H_{234}F_9N_{12}O_{21}Ru_6S_3$ ($[M - 3CF_3SO_3]^{3+}$): *m*/*z* 1246.7. Found: *m*/*z* 1246.7. Calcd for $C_{178}H_{234}F_{12}N_{12}O_{24}Ru_6S_4$ ($[M - 2CF_3SO_3]^{2+}$): *m*/*z* 1944.5. Found: *m*/*z* 1945.1. Elem anal. Calcd for $C_{180}H_{236}F_{18}N_{18}O_{30}Ru_6S_6 \cdot 3CH_2Cl_2$ (4191.0 + 254.78): C, 49.49; H, 5.45; N, 3.78. Found: C, 49.50; H, 5.88; N, 3.39.

■ ASSOCIATED CONTENT

Supporting Information

The Supporting Information is available free of charge on the ACS Publications website at DOI: 10.1021/acs.inorgchem.7b02668.

ESI-MS spectra of all complexes **1**−**2** (PDF)

■ AUTHOR INFORMATION

Corresponding Author

*E-mail: bruno.therrien@unine.ch.

ORCID

Bruno Therrien: 0000-0002-0388-2745

Notes

The authors declare no competing financial interest.

■ REFERENCES

(1) Maeda, H.; Wu, J.; Sawa, T.; Matsumura, Y.; Hori, K. Tumor vascular permeability and the EPR effect in macromolecular therapeutics: a review. *J. Controlled Release* **2000**, *65*, 271−284.

(2) Maeda, H.; Tsukigawa, K.; Fang, J. A Retrospective 30 Years After Discovery of the Enhanced Permeability and Retention Effect of Solid Tumors: Next-Generation Chemotherapeutics and Photodynamic Therapy-Problems, Solutions, and Prospects. *Microcirculation* **2016**, *23*, 173−182.

(3) Danhier, F. To exploit the tumor microenvironment: Since the EPR effect fails in the clinic, what is the future of nanomedicine? *J. Controlled Release* **2016**, *244*, 108−121.

(4) Nasu, R.; Kimura, H.; Akagi, K.; Murata, T.; Tanaka, Y. Blood flow influences vascular growth during tumour angiogenesis. *Br. J. Cancer* **1999**, *79*, 780−786.

(5) Yin, H.; Liao, L.; Jun, F. Enhanced Permeability and Retention (EPR) Effect Based Tumor Targeting: The Concept, Application and Prospect. *JSM Clin. Oncol. Res.* **2014**, *2*, 1010.

(6) Freitas, R. A. *Nanomedicine*; Landes Bioscience: Austin, TX, 1999.

(7) Wang, J.; Lu, Z.; Gao, Y.; Wientjes, M. G.; Au, J. L.-S. Improving delivery and efficacy of nanomedicines in solid tumors: role of tumor priming. *Nanomedicine* **2011**, *6*, 1605−1620.

(8) Yuan, F.; Dellian, M.; Fukumura, D.; Leunig, M.; Berk, D. A.; Torchilin, V. P.; Jain, R. K. Vascular permeability in a human tumor xenograft: molecular size dependence and cutoff size. *Cancer Res.* **1995**, *55*, 3752−3756.

(9) Jain, R. K.; Stylianopoulos, T. Delivering nanomedicine to solid tumors. *Nat. Rev. Clin. Oncol.* **2010**, *7*, 653−664.

(10) Fang, J.; Nakamura, H.; Maeda, H. The EPR effect: Unique features of tumor blood vessels for drug delivery, factors involved, and limitations and augmentation of the effect. *Adv. Drug Delivery Rev.* **2011**, *63*, 136−151.

(11) Suzuki, M.; Hori, K.; Abe, I.; Saito, S.; Sato, H. A New Approach to Cancer Chemotherapy: Selective Enhancement of Tumor Blood Flow With Angiotensin II. *J. Natl. Cancer Inst.* **1981**, *67*, 663−669.

(12) Duncan, R. Polymer conjugates as anticancer nanomedicines. *Nat. Rev. Cancer* **2006**, *6*, 688−701.

(13) Fassas, A.; Anagnostopoulos, A. The use of liposomal daunorubicin (DaunoXome) in acute myeloid leukemia. *Leuk. Lymphoma* **2005**, *46*, 795−802.

(14) European Medicines Agency. Science Medicines Health. Zusammenfassung des EPAR für die Öffentlichkeit: Abraxane, http://www.ema.europa.eu/docs/de_DE/document_library/EPAR_-_Summary_for_the_public/human/000778/WC500020431.pdf.

(15) National Cancer Institute. Paclitaxel-loaded polymeric micelle, https://www.cancer.gov/publications/dictionaries/cancer-drug?cdrid=434427.

(16) European Medicines Agency. Science Medicines, Health: Depocyte, http://www.ema.europa.eu/docs/en_GB/document_library/EPAR_-_Scientific_Discussion/human/000317/WC500035646.pdf.

(17) Barenholz, Y. Doxil — The first FDA-approved nano-drug: Lessons learned. *J. Controlled Release* **2012**, *160*, 117−134.

(18) European Medicines Agency. Science Medicines, Health: Zusammenfassung des EPAR für die Öffentlichkeit: Myocet, http://www.ema.europa.eu/docs/de_DE/document_library/EPAR_-_Summary_for_the_public/human/000297/WC500031806.pdf.

(19) National Cancer Institute. Calaspargasse pegol and pegaspargase, https://www.cancer.gov/publications/dictionaries/cancer-drug?search=oncaspar.

(20) Maeda, H.; Bharate, G. Y.; Daruwalla, J. Polymeric drugs for efficient tumor-targeted drug delivery based on EPR-effect. *Eur. J. Pharm. Biopharm.* **2009**, *71*, 409−419.

(21) Haag, R.; Kratz, F. Polymer Therapeutics: Concepts and Applications. *Angew. Chem., Int. Ed.* **2006**, *45*, 1198−1215.

(22) Kobayashi, H.; Watanabe, R.; Choyke, P. L. Improving Conventional Enhanced Permeability and Retention (EPR) Effects; What Is the Appropriate Target? *Theranostics* **2014**, *4*, 81−89.

(23) Caliceti, P.; Veronese, F. M. Pharmacokinetic and biodistribution properties of poly (ethylene glycol)−protein conjugates. *Adv. Drug Delivery Rev.* **2003**, *55*, 1261−1277.

(24) Therrien, B. Biologically relevant arene ruthenium metalla-assemblies. *CrystEngComm* **2015**, *17*, 484−491.

(25) Therrien, B. Transporting and Shielding Photosensitisers by Using Water-Soluble Organometallic Cages: A New Strategy in Drug Delivery and Photodynamic Therapy. *Chem. - Eur. J.* **2013**, *19*, 8378−8386.

(26) Therrien, B.; Furrer, J. The biological side of water-soluble arene ruthenium assemblies. *Adv. Chem.* **2014**, *2014*, 1−20.

DOI: 10.1021/acs.inorgchem.7b02668
Inorg. Chem. 2018, 57, 3626−3633

(27) Yan, H.; Süss-Fink, G.; Neels, A.; Stoeckli-Evans, H. Mono-, di- and tetra-nuclear *p*-cymeneruthenium complexes containing oxalato ligands. *J. Chem. Soc., Dalton Trans.* **1997**, *22*, 4345−4350.
(28) Singh, A. K.; Pandey, D. S.; Xu, Q.; Braunstein, P. Recent Advances in Supramolecular and Biological Aspects of Arene Ruthenium(II) Complexes. *Coord. Chem. Rev.* **2014**, *270*−*271*, 31−56.
(29) Dubey, A.; Jeong, Y. J.; Jo, J. H.; Woo, S.; Kim, D. H.; Kim, H.; Kang, S. C.; Stang, P. J.; Chi, K.-W. Anticancer Activity and Autophagy Involvement of Self-Assembled Arene-Ruthenium Metallacycles. *Organometallics* **2015**, *34*, 4507−4514.
(30) Mishra, A.; Kang, S. C.; Chi, K.-W. Coordination-Driven Self-Assembly of Arene-Ruthenium Compounds. *Eur. J. Inorg. Chem.* **2013**, *2013*, 5222−5232.
(31) Therrien, B.; Süss-Fink, G.; Govindaswamy, P.; Renfrew, A. K.; Dyson, P. J. The "Complex-in-a-Complex" Cations $[(acac)_2M\subset Ru_6(p\text{-}iPrC_6H_4Me)_6(tpt)_2(dhbq)_3]^{6+}$: A Trojan Horse for Cancer Cells. *Angew. Chem., Int. Ed.* **2008**, *47*, 3773−3776.
(32) Therrien, B. Functionalised η^6-arene ruthenium complexes. *Coord. Chem. Rev.* **2009**, *253*, 493−519.
(33) Barry, N. P. E.; Furrer, J.; Freudenreich, J.; Süss-Fink, G.; Therrien, B. Designing the Host-Guest Properties of Tetranuclear Arene Ruthenium Metalla-Rectangles to Accommodate a Pyrene Molecule. *Eur. J. Inorg. Chem.* **2010**, *5*, 725−728.
(34) Schmitt, F.; Freudenreich, J.; Barry, N. P. E.; Juillerat-Jeanneret, L.; Süss-Fink, G.; Therrien, B. Organometallic Cages as Vehicles for Intracellular Release of Photosensitizers. *J. Am. Chem. Soc.* **2012**, *134*, 754−757.
(35) Yi, J. W.; Barry, N. P. E.; Furrer, M. A.; Zava, O.; Dyson, P. J.; Therrien, B.; Kim, B. H. Delivery of Floxuridine Derivatives to Cancer Cells by Water-Soluble Organometallic Cages. *Bioconjugate Chem.* **2012**, *23*, 461−471.
(36) Pitto-Barry, A.; Barry, N. P. E.; Zava, O.; Deschenaux, R.; Dyson, P. J.; Therrien, B. Double Targeting of Tumours with Pyrenyl-Modified Dendrimers Encapsulated in an Arene-Ruthenium Metallaprism. *Chem. - Eur. J.* **2011**, *17*, 1966−1971.
(37) Pitto-Barry, A.; Barry, N. P. E.; Zava, O.; Deschenaux, R.; Therrien, B. Encapsulation of Pyrene-Functionalized Poly(benzyl ether) Dendrons into a Water-Soluble Organometallic Cage. *Chem. - Asian J.* **2011**, *6*, 1595−1603.
(38) Lu, S.; Drees, M.; Yao, Y.; Boudinet, D.; Yan, H.; Pan, H.; Wang, J.; Li, Y.; Usta, H.; Facchetti, A. 3,6-Dithiophen-2-yldiketopyrrolo[3,2-*b*]pyrrole (isoDPPT) as an Acceptor Building Block for Organic Opto-Electronics. *Macromolecules* **2013**, *46*, 3895−3906.
(39) Chen, F.; Zhang, G.; Hong, Z.; Lin, Z.; Lei, M.; Huang, M.; Hu, L. Design, synthesis, and SAR of embelin analogues as the inhibitors of PAI-1 (plasminogen activator inhibitor-1). *Bioorg. Med. Chem. Lett.* **2014**, *24*, 2379−2382.
(40) Furrer, M. A.; Furrer, J.; Therrien, B. Physical and physicochemical stimuli-responsive arene ruthenium metallaprism. *Organometallics* **2012**, *31*, 3149−3154.
(41) Garci, A.; Dobrov, A. A.; Riedel, T.; Orhan, E.; Dyson, P. J.; Arion, V. B.; Therrien, B. Strategy to Optimize the Biological Activity of Arene Ruthenium Metalla-Assemblies. *Organometallics* **2014**, *33*, 3813−3822.
(42) Garci, A.; Mbakidi, J.-P.; Chaleix, V.; Sol, V.; Orhan, E.; Therrien, B. Tunable Arene Ruthenium Metallaprisms to Transport, Shield, and Release Porphin in Cancer Cells. *Organometallics* **2015**, *34*, 4138−4146.
(43) Lewis, J. E. M.; Gavey, E. L.; Cameron, S. A.; Crowley, J. D. Stimuli-responsive Pd_2L_4 metallosupramolecular cages: towards targeted cisplatin drug delivery. *Chem. Sci.* **2012**, *3*, 778−784.
(44) Schmidt, A.; Molano, V.; Hollering, M.; Pöthig, A.; Casini, A.; Kühn, F. E. Evaluation of new palladium cages as potential delivery systems for the anticancer drug cisplatin. *Chem. - Eur. J.* **2016**, *22*, 2253−2256.
(45) Zheng, Y.-R.; Suntharalingam, K.; Johnstone, T. C.; Lippard, S. J. Encapsulation of Pt(IV) prodrugs within a Pt(II) cage for drug delivery. *Chem. Sci.* **2015**, *6*, 1189−1193.
(46) Stang, P. J. Abiological self-assembly via coordination: Formation of 2D metallacycles and 3D metallacages with well-defined shapes and sizes and their chemistry. *J. Am. Chem. Soc.* **2012**, *134*, 11829−11830.
(47) Bennett, M. A.; Huang, T.-N.; Matheson, T. W.; Smith, A. K.; Ittel, S.; Nickerson, W. (η^6-Hexamethylbenzene)ruthenium Complexes. *Inorg. Synth.* **1982**, *21*, 74−78.
(48) Anderson, H. L.; Anderson, S.; Sanders, J. K. M. Ligand binding by butadiyne-linked porphyrin dimers, trimers and tetramers. *J. Chem. Soc., Perkin Trans. 1* **1995**, *1*, 2231−2246.

DOI: 10.1021/acs.inorgchem.7b02668
Inorg. Chem. 2018, 57, 3626−3633